ADVANCED MATERIALS INTERFACES
www.advmatinterfaces.de

Vertical Integration of Cell-Laden Hydrogels with Bioinspired Photonic Crystal Membranes

*Yi Pei, Sayyed Hamed Shahoei, Yanfen Li, Peter J. Reece, Erik R. Nelson, J. Justin Gooding, and Kristopher A. Kilian**

The native architecture of tissue segregates populations of cells through nanostructured membranes of biopolymers (e.g., basement membranes) which serve the dual purpose of providing scaffolding for cells and filtration through size-exclusion. A multilayered approach to fabricate tissue scaffolds where populations of encapsulated cells are separated by porous silicon (PSi)-based photonic crystal membranes with nano- and microstructure that mimics the basement membranes is reported here. The PSi films are fabricated to display discreet photonic bandgaps such that remote optical interrogation provides a specific resonance for each film. Through careful control of surface chemistry, nanostructured PSi films are engineered to serve as optical biosensors and biomolecule release reservoirs, where the optical signature can report on these distinct functions remotely using a simple light source. The promise of this approach is demonstrated as a "smart" tissue scaffolding by monitoring matrix metalloprotease (MMP) activity from encapsulated multilayered co-cultures of mesenchymal stem cells and human microvascular endothelial cells, with concurrent attenuation of MMP activity through release of angiogenic-modulating compounds. The integration of optically registered biosensing and drug-release capabilities—within a multilayered hydrogel scaffold with multiple cell types—provides a new approach to tissue engineering where dynamic bioactivity can be monitored remotely in real-time.

A paradigm in tissue engineering is the design of scaffolding that recapitulates the architecture of native tissue for integration with live cells and restoration of function.[1] A key structural aspect of most solid tissues is the presence of membranes that serve a dual function of promoting cell adhesion and organization, and for size-exclusion filtration to modulate diffusion between compartments. The integration of biopolymeric membrane structures within tissue engineering scaffolds has been demonstrated through the development of fibrous mats prepared via methods including electrospinning of matrix protein,[2] layer-by-layer deposition,[3] 3D bioprinting,[4] or through guiding the native tendency of cells to synthesize matrix in vitro.[5]

A challenge to the field of tissue engineering is the inherent difficulty with monitoring cell–matrix interactions once the cell-laden scaffold is fabricated, thereby necessitating cell fixation and sectioning to evaluate integration of discreet cell types within the scaffold materials. A common strategy to address this challenge

Y. Pei
Department of Materials Science and Engineering
University of Illinois at Urbana-Champaign
Urbana, IL 61801, USA

S. H. Shahoei
Department of Molecular and Integrative Physiology
University of Illinois at Urbana-Champaign
Urbana, IL 61801, USA

Dr. Y. Li
Department of Biomedical & Nutritional Sciences
University of Massachusetts Lowell
Lowell, MA 01854, USA

Dr. P. J. Reece
School of Physics
University of New South Wales
Sydney, NSW 2052, Australia

The ORCID identification number(s) for the author(s) of this article can be found under https://doi.org/10.1002/admi.201801233.

DOI: 10.1002/admi.201801233

Prof. E. R. Nelson
Department of Bioengineering
University of Illinois at Urbana-Champaign
Urbana, IL 61801, USA

Prof. J. J. Gooding
School of Chemistry
Australian Centre for Nanomedicine
ARC Centre of Excellence in Convergent Bio-Nano Science and Technology
University of New South Wales
Sydney, NSW 2052, Australia

Prof. K. A. Kilian
School of Chemistry
School of Materials Science and Engineering
Australian Centre for Nanomedicine
University of New South Wales
Sydney, NSW 2052, Australia
E-mail: k.kilian@unsw.edu.au

is labelling the cells with a fluorescent reporter to track integration using various live cell and tissue imaging approaches.[6] In addition, researchers have incorporated various sensing materials within tissue-engineered materials to monitor cell integration including fluorescence reporters,[7,8] nanoparticle probes,[9,10] graphene films,[11] and electronic circuits.[12,13] However, there are significant limitations to these approaches, where cell division leads to loss of fluorescent signals, and homogenous sensing materials suffer from lack of specificity and limitations with remote transduction.

In this communication, we demonstrate a new approach to tissue engineering where optically encoded thin films are integrated with cell-laden hydrogel materials. Porous silicon (PSi) photonic crystals are designed to emulate the nano- and microarchitecture of membranes in biology, with distinct spectral codes and complementary functionalities including: 1) biosensing of cell-secreted enzymes, and 2) release of bioactive compounds. These optical biomaterials are vertically integrated via transfer printing with hydrogels containing mesenchymal stem cells (MSCs) and human microvascular endothelial cells (hMVECs) as a prototypical heterotypic multilayered tissue construct (**Scheme 1**).

PSi shows broad potential as a material for application in biotechnology and biomedicine,[14] with a number of important characteristics for integration with biological systems, such as biocompatibility,[15] biodegradability,[16] ease of fabrication,[17] well-established chemical modification methods,[18,19] porous structure for drug and growth factor loading,[20] and tunable optical properties.[21] PSi is fabricated by electrochemical etching of single crystal silicon in hydrofluoric acid (HF) solution. Different PSi-based photonic crystals have been fabricated including distributed Bragg reflectors (DBR),[22,23] resonant microcavities,[24,25] and rugate filters[26,27] by programing the current density during the electrochemical etching process. PSi is sensitive to changes in the refractive index within the nanoporous architecture, which has led to significant research in using PSi materials for biosensing.[28]

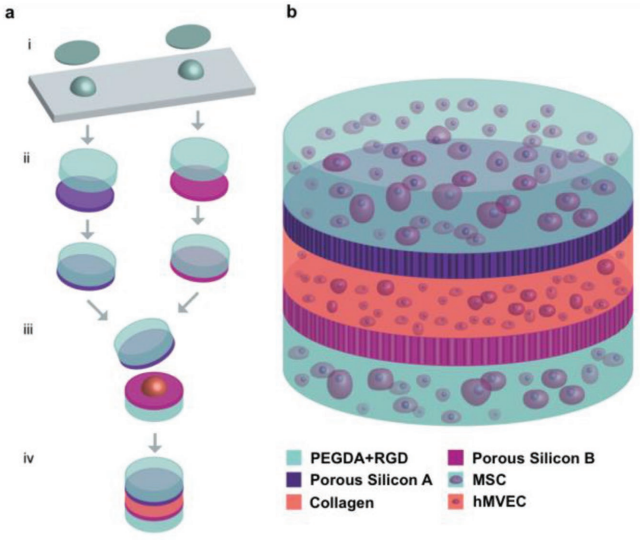

Scheme 1. a) The fabrication process and b) the structure of the multilayered 3D scaffold.

Rugate filters were formed by electrochemical etching of p-type silicon in ethanolic HF solution through a programmed sinusoidal current density; etching parameters were optimized to yield a film with average pore size of 60+/–20 nm (Figure S1, Supporting Information) and a tunable film thickness from hundreds of nanometers to tens of microns.[29] To ensure high reflectivity of the stopband, we fabricated films with thickness of 12–15 µm. Importantly, this range of pore dimensions and membrane thickness can be tuned to align with the average pore diameter and thickness of basement membranes in many tissues.[30] Figure S2 in the Supporting Information shows an example of thinner PSi films that can be fabricated. PSi is rapidly oxidized in biological media and therefore needs to be passivated with a suitable surface chemistry.[31] Researchers have developed numerous chemical modification strategies to passivate PSi and to enable distal bioconjugation.[32] Here we performed hydrosilylation of 10-undecenoic acid, which has a terminal carboxylic acid group that can be used for further conjugation of biomolecules. **Figure 1**a depicts the derivatization steps and Figure 1b shows spectra collected using Fourier transform infrared spectroscopy (FTIR). Freshly etched PSi surfaces are dominated by silicon hydride stretching Si-H_x (x = 1,2,3) at 2100 cm^{-1}. Thermal hydrosilylation of neat 10-undecenoic acid leads to a decrease in Si-H_x modes and the appearance of C-H (≈2930 cm^{-1}) and C=O (≈1714 cm^{-1}) stretching modes indicating successful functionalization (Figure 1b). The terminal carboxylic acid groups were activated by ethyl(dimethylaminopropyl)carbodiimide (EDC)/N-Hydroxysuccinimide (NHS) chemistry which leads to a shift in the carbonyl C=O stretch (1740 cm^{-1}) and appearance of succinimidyl C=O stretching at 1815 and 1786 cm^{-1}. To provide a biorecognition interface for detection of matrix metalloprotease (MMP) activity from cells, we used our previously reported method of immobilization of gelatin hydrogel material within the pore space,[33] to serve as a substrate for secreted MMP-2 and MMP-9. Gelatin integration is indicated by the appearance of amide I (≈1643 cm^{-1}) and amide II (≈1543 cm^{-1}) bands as shown in Figure 1b. The PSi films were removed from the substrate using a short sequence of electrochemical pulses to electropolish at the base before chemical modifications; mechanical scribing at the perimeter led to release of the thin film.

The optical properties of the PSi films were assessed during derivatization using reflectivity spectroscopy. Freshly etched PSi rugate filters were constructed to have a high reflectivity stopband in the "tissue-window" near-IR region toward remote monitoring through integrated tissue scaffolds. Figure 1c shows the rugate filter resonance at 748 nm, which shifts 36 nm to 784 nm after hydrosilylation of 10-undecenoic acid, and an additional 10 to 794 nm after EDC/NHS treatment. These shifts indicate that air in the pore space is replaced by organic material of a higher refractive index. After the sample is impregnated with gelatin and dried, the stopband shows a large shift to 860 nm, suggesting that a considerable quantity of pore space is occupied by gelatin. This is important for biosensing to ensure sensitivity to MMP activity as the gelatin is digested within the pore space leading to a blue shift in the resonance position.

To integrate the chemically modified PSi into a 3D scaffold, we investigated a multilayer vertical integration approach based on transfer printing.[25] To evaluate the versatility of the

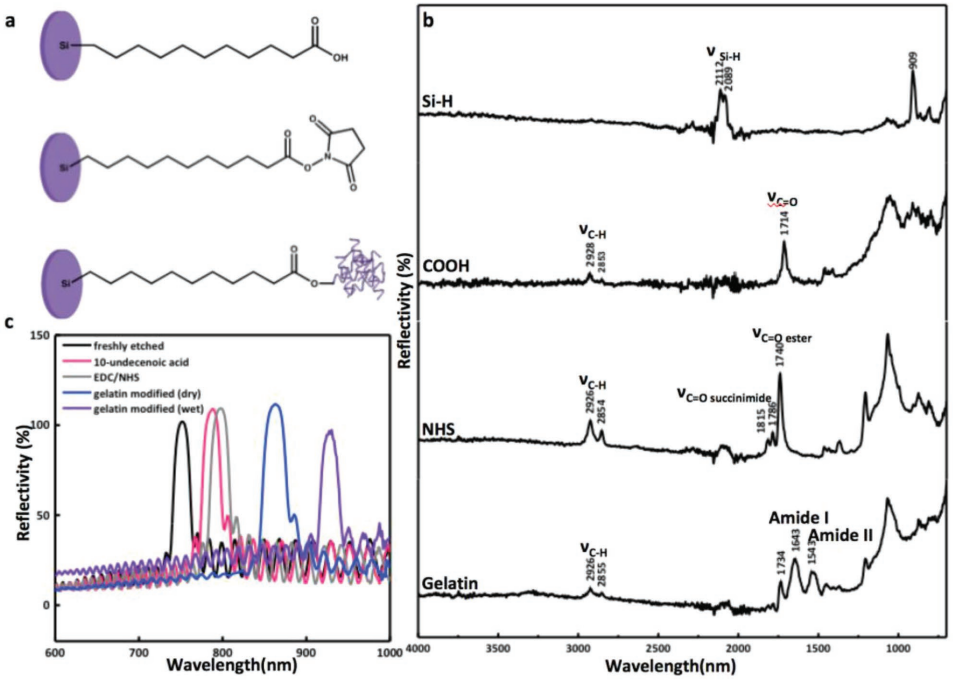

Figure 1. Chemical modifications of PSi. a) Scheme of modification steps. b) FTIR data of PSi after each modification step. c) Reflectivity spectra of PSi rugate filter after each modification step.

approach, we chose to use two common hydrogels utilized for tissue engineering: synthetic polyethylene glycol diacrylate (PEGDA) for its tunable mechanical properties, and natural collagen I for its ability to support cell attachment and growth. PEGDA was made by acrylation of polyethylene glycol (PEG) with a percentage derivatization of 87% (Figure S3, Supporting Information). To encourage cell adhesion and interaction within the PEGDA hydrogel matrix and better restore the native microenvironment, the minimum binding sequence from fibronectin, Arg-Gly-Asp (RGD), was conjugated to PEGDA through Michael addition of the terminal/cysteine of Cys-Gly-Arg-Gly-Asp-Ser (CG*RGD*S).[34] At pH 8, the Michael addition reaction is favored; however, we cannot discount the possibility of some moderate ester hydrolysis within the hydrogel under these conditions. CG*RGD*S peptide was made by solid-phase peptide synthesis (SPPS) method and was verified by mass spectrometry (Figure S4, Supporting Information). Based on our previous study, the presence of MSCs greatly increases tube formation of hMVECs,[35] which has the potential to be utilized to help with wound healing process. Therefore, we encapsulated both cell types in the multilayered 3D scaffold with the expectation to gain better understanding of the interactions between the cells.

The procedure for fabricating the multilayer scaffold is shown in Scheme 1: 1) formation of PEGDA+RGD gel layers with encapsulated cells on silanized coverslips; 2) transfer printing of freestanding PSi films to the gel; and 3) the casting of a second cell-laden hydrogel layer. Transfer printing is a set of techniques for assembly of micro-/nanomaterials by modulating the physical adhesion between different interfaces[36]; subtractive transfer, as we used in our experiment, is one type of transfer method that utilizes a stamp to selectively pick up regions of a donor film.[37] In this way, additional layers can be casted and PSi films transfer printed to reach the desired architecture. **Figure 2**a shows a cross-sectional scanning

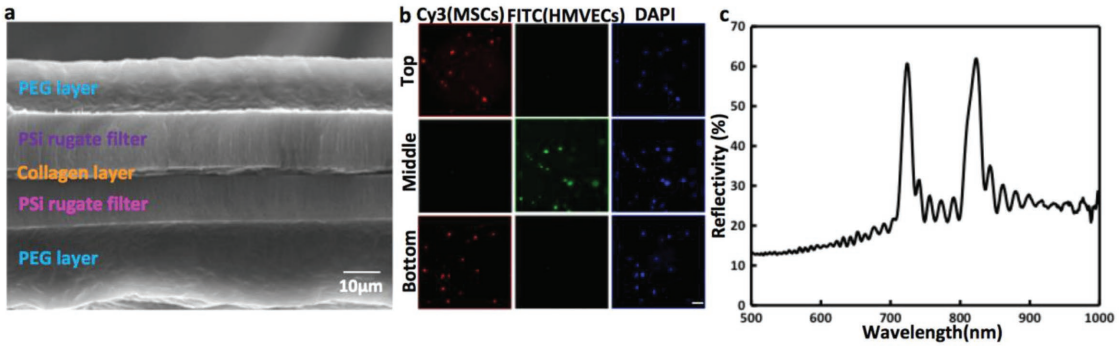

Figure 2. a) Cross-sectional SEM image of the multilayered 3D scaffold. b) Fluorescence images of the different hydrogel layers (scale bar represents 100 μm). c) Reflectivity spectrum of the multilayered 3D scaffold.

electron microscope (SEM) image of a multilayer structure consisting of PEGDA:PSi1:ColI:PSi2:PEGDA, indicating the successful fabrication of the photonic scaffold. The top and bottom layers are PEGDA gels with a thickness of 15–20 μm. The two PSi films are adjacent to PEGDA layers with a thickness of 12–15 μm. The thin layer in the middle is made of collagen and has a thickness of about 3 μm. Note that the thickness of hydrogels can be readily tuned by adjusting the amount of hydrogel solution applied, and silicon-based photonic films can be fabricated with thickness ranging from hundreds of nanometers to tens of microns. The apparent thickness of the collagen layer is because of collapse during SEM vacuum conditions; microscopy of the hydrated architecture demonstrates comparable dimensions to the PEGDA hydrogels as shown in Figure S5 in the Supporting Information. Prior to encapsulation, the MSCs were treated with CellTracker Red CMTPX, and the hMVECs were treated with CellTracker Green CMFDA in order to visualize the cells in the layered structure. Fluorescence images of the different hydrogel layers were acquired to verify the encapsulation of cells and the correct spatial distribution (Figure 2b). Fluorescence confirms cell viability in all layers; MSCs are present in both top and bottom PEGDA hydrogel layers while hMVECs only reside in the central collagen I layer. This result demonstrates that cells can be effectively encapsulated in different gel layers, interspersed between PSi films.

Our aim is to develop a multilayered tissue scaffold where each film can be optically interrogated simultaneously. Therefore, the two PSi films were engineered to display different stopbands, one at 720 nm and the other at 820 nm. Reflectivity spectroscopy reveals two distinct peaks corresponding to the two different PSi films (Figure 2c), indicating that the signature optical properties of both PSi films are successfully maintained and can be detected in one measurement. Moreover, the positions of the peaks are completely independent from each other, providing the opportunity to use multiple PSi films for varied functionalities (e.g., biosensing and drug release).

Several groups have demonstrated the use of PSi optical structures for detecting the activity of protease enzymes.[33,38,39] To evaluate the utility of PSi sensors for in situ monitoring of MMPs secreted from encapsulated cells, two PEGDA layers containing MSCs and hMVECs were assembled on top of the PSi sensor. Control samples were included with PEGDA hydrogel layers without cells; experimental groups contained encapsulated MSCs, hMVECs, and both MSCs+hMVECs. The cells were cultured for 24 h and the reflectivity spectra of PSi sensors were measured both before and after cell culture. The blue shift in the stopband was calculated for each PSi sensor at 24 h: $\Delta\lambda = \lambda_{0\ h} - \lambda_{24\ h}$, with $\Delta\lambda > 0$ indicating blue shifts. To control for blue shifts caused by PSi oxidation in aqueous environments and potential gelatin dissolution unrelated to cell activities, the experimental group was normalized to the control group: $\Delta\lambda_{normalized} = \Delta\lambda_{experimental} - \Delta\lambda_{control}$, with $\Delta\lambda_{normalized} > 0$ indicating blue shifts associated with degradation of gelatin corresponding to MMP activity. For MSCs alone or when co-cultured with hMVECs, there is a blue shift $\Delta\lambda_{normalized}$ on the order of 5–15 nm, indicating a change in the pore space refractive index, which suggests the presence of secreted active MMPs (**Figure 3**a). However, hMVECs alone led to red shift suggesting limited gelatinolytic activity and the domination of endogenous release of other proteins that were physically absorbed into PSi pores and increased the average refractive index of the structure. We used gelatin zymography to verify that the optical readout from the PSi films was on account of MMPs. Conditioned media was collected from MSCs,

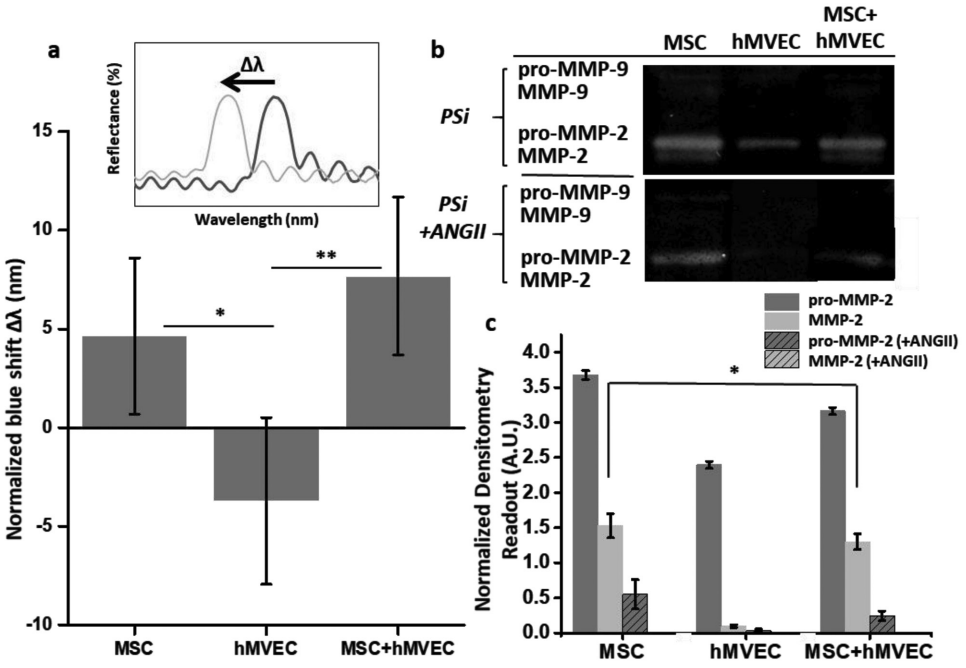

Figure 3. a) Representative blue shift in spectra after gelatin digestion in PSi; normalized blue shift after 24 h culture with MSC, hMVEC, and MSC+hMVEC. b,c) Gelatin zymography data of the conditioned media collected from MSC, hMVEC, and MSC+hMVEC after 24 h culture w/ and w/o ANGII. Error bars represent standard deviation of 5 replicate measurements. *p-value 0.05 **p-value 0.001.

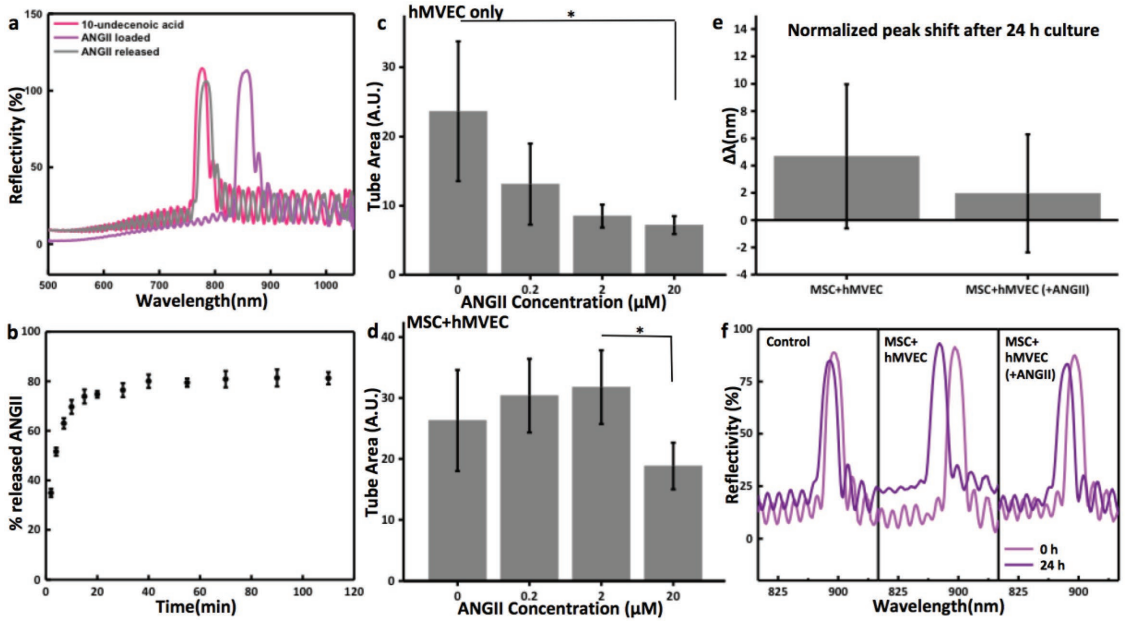

Figure 4. a) Reflectivity spectra of PSi rugate filter before loading ANGII, after loading ANGII, and after ANGII release. b) ANGII release profile. c,d) Effect of ANGII on hMVEC tube formation. e) Normalized blue shift after 24 h culture with MSC+hMVEC w/ and w/o ANGII. f) Blue shift of PSi stopbands when cultured without cells, with MSC+hMVEC, and with MSC+hMVEC+ANGII. Error bars represent standard deviation of 5 replicate measurements. *p-value 0.05.

HMVECs, and MSCs+HMVECs and then loaded on gelatin zymography gels (Figure 3b,c). Consistent with the biosensor results, we see the same trend in active MMP-2 secreted from MSCs and MSCs+HMVECs, with lower activity from HMVECs (Figure 3c). There was a very low level of MMP-9 under all conditions (at detection limits) (Figures S6 and S7, Supporting Information) that could not be quantitated.

Another attribute of PSi is the potential for sustained release of drugs and other compounds.[40,41] To explore the use of PSi films for biomolecule release, we loaded the angiogenic modulator angiotensin II (ANGII) into a PSi film by wetting the pore space with ethanolic solution (1×10^{-3} M; 50% ethanol (v/v)), followed by evaporation and drying. After treating the PSi with ANGII, the reflectivity spectra show a significant red shift of 76 nm, indicating successful incorporation into the pores of PSi (**Figure 4**a). The ANGII-loaded sample was placed in buffer at 37 °C and the concentration of ANGII released was monitored over time by UV–Vis spectroscopy. Under these conditions, ANGII shows an initial burst release from the PSi of ≈80% within 60 min (Figure 4b). Concurrently, the reflectivity spectra blue shifted 72 nm compared to the initial 80 nm red shift, serving as an optical indication of drug release (Figure 4a). It is reasonable to speculate that some ANGII remains confined within the nanoporous architecture, and will slowly diffuse from the thin film over prolonged times during passive oxidation of PSi. Tuning the porosity and the surface chemistry will allow engineering the drug release characteristics to match the desired bioactivity.[20] To investigate a functional outcome of the ANGII release, we employed a model angiogenesis assay based on endothelial tubulogenesis.[35] Matrigel, a 3D hydrogel commonly used in tissue engineering, was formed on the surface of ANGII-loaded PSi films. At all concentrations, ANGII inhibited tubulogenesis in hMVECs within the hydrogel (Figure 4c). This is consistent with previous finding that ANGII can inhibit vascular endothelial growth factor (VEGF)-induced hMVEC tube formation by stimulating angiotensin type 2 (AT_2) receptor.[42] Interestingly, when MSCs were co-cultured with hMVECs, we see less inhibition of tubulogenesis suggesting proangiogenic secretion from MSCs as observed previously[35] (Figure 4d). Moreover, gelatin zymography shows that treatment of cells with ANGII leads to a precipitous drop in secreted MMPs, particularly the active forms (Figure 3b,c). This observation is consistent with the response of PSi sensor as shown in Figure 4e,f. Taken together, these results demonstrate that PSi films can be used as bioactive molecule reservoirs to modulate the activity and secretory profile of surrounding cells in the scaffold.

In summary, we have shown how PSi optical materials can be vertically integrated with cell-laden hydrogel biomaterials using a transfer printing approach. Tuning the thickness of different layers allow us to better mimic the native architectures of multilayered tissue, and the photonic properties of PSi enable real-time monitoring of cellular secretion from one film, with simultaneous biomolecular release from the second film. In this way, dynamic feedback mechanisms can be incorporated into spectrally distinct thin films, to impart dynamic properties to surrounding populations of cells. We demonstrated this concept by monitoring MMP release from mixed populations of MSCs and hMVECs, with concurrent release of the angiogenic peptide ANGII. This new approach will allow incorporation of any mixture of cell types, with virtually any soft biomaterial, with the integration of multiple spectrally distinct optical films tuned for a range of functionalities including: growth monitoring, biosensing, sequestration, and tunable molecular release. This approach is expected to show wide versatility in

tissue engineering for developing optically encoded dynamic multilayered tissues.

Experimental Section

Materials: Reagents were purchased from Sigma-Aldrich unless otherwise noted. Human MSCs (Lonza) tested positive for CD105, CD166, CD29, and CD44, negative for CD14, CD34, and CD45 by flow cytometry. Growth factor reduced basement membrane extract (matrigel) was purchased from Trevigen. hMVECs were purchased from Cell Systems. EGM-2 growth factor supplemented media was purchased from Lonza.

Cell Source and Culture: MSCs were cultured in low glucose (1 g mL^{-1}), Dulbecco's modified Eagle medium (DMEM) (10% FBS and 1% penicillin/streptomycin), and hMVECs were cultured in EGM-2 media. Cells were passaged at ≈80% confluency and media was changed every 3–4 days. Trypsinization of adherent cells involved dissociation in 0.25% Trypsin or 0.05% Trypsin followed by seeding at ≈5000 cells cm^{-2}.

Solid-Phase Peptide Synthesis: CGRGDS peptide was synthesized using Fmoc SPPS. N-terminal fluorenylmethyloxycarbonyl (Fmoc) protected rink amide resin was deprotected in 20% piperidine in N′,N′-dimethylformamide (DMF) and washed with DMF. Benzotriazol-1-yl-oxytripyrrolidinophosphonium hexafluorophosphate (PyBOP), and N-methylmorpholine in DMF was added to three equivalents of amino acid for 2 h at room temperature for each additional amino acid. Peptide was cleaved by stirring in 95% trifluoroacetic acid (TFA), 2.5% H_2O, and 2.5% triisopropylsilane (TIS) for 2 h and precipitated in cold diethyl ether followed by lyophilization. Peptides were analyzed by mass spectrometry (electrospray ionization (ESI)).

Porous Silicon Fabrication: Si (100) wafers (p-type, B-doped, 0.005 ohm cm) were immersed in an electrochemical cell containing 1:1 aqueous HF (48%) and ethanol, with a platinum wire electrode and steel electrode contacting the back. Rugate filters were etched using a sinusoidally varying current density alternating between 370 and 430 mA using a SP-200 BioLogic Galvanostat. After etching PSi was washed in ethanol for three times, and then dried under nitrogen. For fabricating free-standing PSi films, a short high current pulse was applied within the etching cell.

PSi Chemical Modification: Hydrosilylation of neat undecenoic acid, subjected to 5 times freeze–pump–thaw cycles under an argon atmosphere, was performed in the presence of freshly etched PSi. Terminal carboxylic acids were activated using 0.1 M EDC with NHS in acetonitrile. Gelatin (Type A; from Procine skin) was dissolved in distilled water to make a high concentration (200 mg mL^{-1}) solution. Hundred microliter solution was casted on top of one PSi film and put under 37 °C for 1 h for conjugation of gelatin. The sample was then moved to 4 °C and let dry.

PEGDA Hydrogel Fabrication: PEG (10 000 molecular weight; 1 mmol) was dried by codistillation with toluene followed by dissolution in dichloromethane (DCM) and toluene (DCM:toluene 5:3). Triethylamine and acryloyl chloride (3 mmol each) were added with stirring under an inert atmosphere, and allowed to react overnight at room temperature. K_2CO_3 was added to the solution with stirring for 1 h. Afterwards, PEGDA reaction solution was filtered, concentrated under vacuum, precipitated in ether, lyophilized, and analyzed by nuclear magnetic resonance (NMR) spectroscopy. PEGDA and CGRGDS peptide (mole ratio 1:1) was then dissolved in 100×10^{-3} M sodium phosphate buffer (pH = 8). The solution was stirred at room temperature for 96 h for the completed Michael addition. After the reaction was done, the polymer was washed and concentrated by spinning in Amicon Ultra-4 10K Centrifugal Filter Unit at 4000 g for 20 min. The polymer was then resuspended in phosphate-buffered saline (PBS) to make to 15 wt% solution. To make hydrogel films, 18 mm glass coverslips (Fischer Scientific) were cleaned, dried, and activated by treatment with 3-(trimethoxysilyl)propyl methacrylate 20% solution in ethanol with 0.3% glacial acetic acid. A 15 wt% solution of PEGDA+CGRGDS and 0.05% 2-Hydroxy-4′-(2-hydroxyethoxy)-2-methylpropiophenone (UV Initiator) was aliquoted to the activated coverslip and applied to a hydrophobic (RainX) treated glass microscope slide. This sandwich was placed in a UV crosslinker (Spectronics) and subjected to UV light at an intensity of ≈5 mW cm^{-2} for 6 min. The coverslip was then lifted up by a pair of tweezers with PEGDA gel attached to the surface.

Transfer Printing of PSi Film: PEGDA gel was used as a stamp and the electropolished PSi film the "ink." PEGDA gel was placed face down onto the PSi film and a pair of tweezers was used to tap on the coverslip in order to ensure a close contact between PEGDA gel and the PSi film. The coverslip was then lifted with PEGDA gel attached to the surface and PSi film attached to PEGDA gel.

Collagen Hydrogel Fabrication: Collagen stock solution from fish scales (provided by Nathan Gabrielson, Materials Science and Engineering, University of Illinois) was neutralized by 1×10^{-3} M NaOH when kept on ice. The neutralized solution was then aliquoted on top of the PSi film that was picked up by PEGDA gel layer. Another PSi film attached PEGDA gel layer was then applied on top of the aliquot. The collagen layer was allowed to gel for 30 min at 37 °C.

Encapsulation of Cells: For cell-laden hydrogel fabrication, MSCs and hMVECs were trypsinized, pelleted, and resuspended in the gel solution prior to polymerization. To confirm cell encapsulation, MSCs were incubated for 30 min with CellTracker Red CMTPX and hMVECs were incubated for 30 min with CellTracker Green CMFDA as per manufacturer's instructions prior to encapsulation. The labeled cells were pelleted and excess cell tracker disposed of.

UV–Vis Spectra: The fixed samples were mounted on glass slides and the reflectivity data were collected by a Zeiss Axio Observer D1 inverted microscope with a 10× objective lens. The measurements were spatially resolved and the spot size used was 0.5 mm. The spectra of five adjacent spots on each sample were collected.

hMVEC Tubulogenesis Assay under the Influence of ANGII: PSi films were loaded with different amount of ANGII and placed on the bottom of a 24 well plate. Two hundred microliter of thawed reduced growth factor matrigel (Trevigen) was coated on top each PSi film and allowed to gel for 30 min at 37 °C. For hMVECs, only system 30000 hMVECs were seeded per well in 500 µL of EBM-2 media with growth factors (Lonza). For the coculture system, 30000 hMVECs and 30000 MSCs were seeded per well in the mixture of 250 µL of EBM-2 media with growth factors and 250 µL of low glucose DMEM. Unsupplemented EBM-2 media was used as a negative control. After 8 h, tube formation was imaged using a Rebel T3 Camera (Canon) at 25× and tube area quantified with imageJ.

Gelatin Zymography: Culture medium was changed to medium without serum 24 h prior to harvest. Conditioned medium was collected, spun at 1000 rpm for 5 min to remove debris. Supernatant was concentrated 20 times using Amicon ultracentrifugal units (Millipore) according to the manufacturer's instructions. Resulting protein concentration was determined by BCA assay and 10 µg of protein was separated on a gelatin-impregnated polyacrylamide gel (Biorad). Gels were washed in Triton X-100/Tris/CaCl2/ZnCl2 buffer briefly to renature proteins, followed by incubation in the same buffer overnight at 37 °C to allow for degradation of gelatin by matrix metalloproteinases. Gels were stained with Coomassie Blue dissolved in methanol/acetic acid solution and destained with methanol/acetic acid solution. Gels were imaged on a Gel Doc system (Biorad) and quantified using Image Studio software (LI-COR).

Characterization Instrumentation: SEM was performed using a JEOL 6060LV General Purpose SEM and a Hitachi S4700 FEG SEM. Reflectivity data were gathered using a Zeiss Axio Observer D1 inverted microscope. PerkinElmer 100 serial FTIR spectrophotometer was used for infrared spectra measurements on samples. NMR data were collected by using Bruker Avance III 600 MHz Cryo NMR. MS data were collected by using Waters Synapt G2-Si ESI/LC-MS. MSCs and hMVECs were imaged using an INCell Analyzer 2000 (GE).

Supporting Information

Supporting Information is available from the Wiley Online Library or from the author.

Acknowledgements

This work was supported by the National Science Foundation Grant 1454616. E.R.N. was supported by the National Cancer Institute of the National Institutes of Health Grant R00CA172357.

Conflict of Interest

The authors declare no conflict of interest.

Keywords

biosensor, drug release, photonic crystals, porous silicon, tissue engineering

Received: August 12, 2018
Revised: October 7, 2018
Published online: October 29, 2018

[1] L. G. Griffith, G. Naughton, *Science* **2002**, *295*, 1009.
[2] X. Wang, B. Ding, B. Li, *Mater. Today* **2013**, *16*, 229.
[3] C. Monge, J. Almodóvar, T. Boudou, C. Picart, *Adv. Healthcare Mater.* **2015**, *4*, 811.
[4] D. Singh, D. Singh, S. S. Han, *Polymers* **2016**, *8*, 19.
[5] G. D. Duraine, W. E. Brown, J. C. Hu, K. A. Athanasiou, *Ann. Biomed. Eng.* **2015**, *43*, 543.
[6] K. M. Dean, A. E. Palmer, *Nat. Chem. Biol.* **2014**, *10*, 512.
[7] Y. J. Heo, H. Shibata, T. Okitsu, T. Kawanishi, S. Takeuchi, *Proc. Natl. Acad. Sci. U. S. A.* **2011**, *108*, 13399.
[8] Y. Chang, Z. Liu, Y. Zhang, K. Galior, J. Yang, K. Salaita, *J. Am. Chem. Soc.* **2016**, *138*, 2901.
[9] X. Zhang, S. Ding, S. Cao, A. Zhu, G. Shi, *Biosens. Bioelectron.* **2016**, *80*, 315.
[10] Y. Dong, M. Lin, G. Jin, Y. Il Park, M. Qiu, Y. Zhao, H. Yang, A. Li, T. Jian Lu, *Nanotechnology* **2017**, *28*, 175702.
[11] H. S. Song, O. S. Kwon, J. H. Kim, J. Conde, N. Artzi, *Biosens. Bioelectron.* **2017**, *89*, 187.
[12] D.-H. Kim, N. Lu, R. Ma, Y.-S. Kim, R.-H. Kim, S. Wang, J. Wu, S. Min Won, H. Tao, A. Islam, K. Jun Yu, T. Kim, R. Chowdhury, M. Ying, L. Xu, M. Li, H.-J. Chung, H. Keum, M. McCormick, P. Liu, Y.-W. Zhang, F. G. Omenetto, Y. Huang, T. Coleman, J. A. Rogers, *Science* **2011**, *333*, 838.
[13] M. S. Mannoor, Z. Jiang, T. James, Y. L. Kong, K. A. Malatesta, W. O. Soboyejo, N. Verma, D. H. Gracias, M. C. McAlpine, *Nano Lett.* **2013**, *13*, 2634.
[14] F. A. Harraz, *Sens. Actuators, B* **2014**, *202*, 897.
[15] M.-A. Shahbazi, M. Hamidi, E. M. Mäkilä, H. Zhang, P. V Almeida, M. Kaasalainen, J. J. Salonen, J. T. Hirvonen, H. A. Santos, *Biomaterials* **2013**, *34*, 7776.
[16] C. Chiappini, X. Liu, J. R. Fakhoury, M. Ferrari, *Adv. Funct. Mater.* **2010**, *20*, 2231.
[17] V. Lehmann, U. Gösele, *Appl. Phys. Lett.* **1991**, *58*, 856.
[18] T. Böcking, K. A. Kilian, K. Gaus, J. J. Gooding, *Adv. Funct. Mater.* **2008**, *18*, 3827.
[19] B. Gupta, Y. Zhu, B. Guan, P. J. Reece, J. J. Gooding, *Analyst* **2013**, *138*, 3593.
[20] E. J. Anglin, L. Cheng, W. R. Freeman, M. J. Sailor, *Adv. Drug Delivery Rev.* **2008**, *60*, 1266.
[21] A. G. Cullis, L. T. Canham, P. D. J. Calcott, *J. Appl. Phys.* **1997**, *82*, 909.
[22] E. Guillermain, V. Lysenko, R. Orobtchouk, T. Benyattou, S. Roux, A. Pillonnet, P. Perriat, *Appl. Phys. Lett.* **2007**, *90*, 241116.
[23] N. H. Maniya, S. R. Patel, Z. V. P. Murthy, *Optik* **2014**, *125*, 828.
[24] S. Chan, Y. Li, L. J. Rothberg, B. L. Miller, P. M. Fauchet, *Mater. Sci. Eng., C* **2001**, *15*, 277.
[25] H. Ning, N. A. Krueger, X. Sheng, H. Keum, C. Zhang, K. D. Choquette, X. Li, S. Kim, J. A. Rogers, P. V. Braun, *ACS Photonics* **2014**, *1*, 1144.
[26] S. Ilyas, T. Böcking, K. Kilian, P. J. Reece, J. Gooding, K. Gaus, M. Gal, *Opt. Mater.* **2007**, *29*, 619.
[27] C. Pacholski, *Sensors* **2013**, *13*, 4694.
[28] A. Jane, R. Dronov, A. Hodges, N. H. Voelcker, *Trends Biotechnol.* **2009**, *27*, 230.
[29] T. Böcking, K. A. Kilian, P. J. Reece, K. Gaus, M. Gal, J. J. Gooding, *ACS Appl. Mater. Interfaces* **2010**, *2*, 3270.
[30] S. J. Liliensiek, P. Nealey, C. J. Murphy, *Tissue Eng., Part A* **2009**, *15*, 2643.
[31] K. A. Kilian, T. Böcking, K. Gaus, M. Gal, J. J. Gooding, *Biomaterials* **2007**, *28*, 3055.
[32] K. A. Kilian, T. Böcking, J. J. Gooding, *Chem. Commun.* **2009**, 630.
[33] K. A. Kilian, L. M. H. Lai, A. Magenau, S. Cartland, T. Böcking, N. Di Girolamo, M. Gal, K. Gaus, J. J. Gooding, *Nano Lett.* **2009**, *9*, 2021.
[34] J. S. Miller, C. J. Shen, W. R. Legant, J. D. Baranski, B. L. Blakely, C. S. Chen, *Biomaterials* **2010**, *31*, 3736.
[35] A. A. Abdeen, J. Lee, S. H. Mo, K. A. Kilian, *J. Mater. Chem. B* **2015**, *3*, 7896.
[36] A. Carlson, A. M. Bowen, Y. Huang, R. G. Nuzzo, J. A. Rogers, *Adv. Mater.* **2012**, *24*, 5284.
[37] D. J. Sirbuly, G. M. Lowman, B. Scott, G. D. Stucky, S. K. Buratto, *Adv. Mater.* **2003**, *15*, 149.
[38] A. H. Soeriyadi, B. Gupta, P. J. Reece, J. J. Gooding, *Polym. Chem.* **2014**, *5*, 2333.
[39] F. S. H. Krismastuti, A. Cavallaro, B. Prieto-Simon, N. H. Voelcker, *Adv. Sci.* **2016**, *3*, 1500383.
[40] C. T. Turner, M. Hasanzadeh Kafshgari, E. Melville, B. Delalat, F. Harding, E. Ma, J. J. Salonen, A. J. Cowin, N. H. Voelcker, *ACS Biomater. Sci. Eng.* **2016**, *2*, 2339.
[41] X. Chen, F. Wo, Y. Jin, J. Tan, Y. Lai, J. Wu, *ACS Nano* **2017**, *11*, 7938.
[42] R. Benndorf, H. B. Rainer, S. Ergün, A. Steenpass, T. Wieland, *Circ. Res.* **1998**, *82*, 619.

